Journal of Colloid and Interface Science 494 (2017) 345–354

Contents lists available at ScienceDirect

Journal of Colloid and Interface Science

journal homepage: www.elsevier.com/locate/jcis

Albumin-mediated deposition of bone-like apatite onto nano-sized surfaces: Effect of surface reactivity and interfacial hydration

Noelia L. D'Elia [a,*,1], Noel Gravina [a,1], Juan M. Ruso [b], Jose L. Marco-Brown [c], Juan M. Sieben [d], Paula V. Messina [a]

[a] Department of Chemistry, Universidad Nacional del Sur, INQUISUR-CONICET, B8000CPB Bahía Blanca, Argentina
[b] Soft Matter and Molecular Biophysics Group, Department of Applied Physics, University of Santiago de Compostela, 15782 Santiago de Compostela, Spain
[c] Environmental Research and Engineering Institute, CONICET, Universidad de San Martín, B1650HMP San Martín, Argentina
[d] Instituto de Ingeniería Electroquímica y Corrosión, INIEC-CONICET, Universidad Nacional del Sur, B8000CPB Bahía Blanca, Argentina

GRAPHICAL ABSTRACT

ARTICLE INFO

Article history:
Received 2 November 2016
Revised 12 January 2017
Accepted 13 January 2017
Available online 16 January 2017

Keywords:
Bovine serum albumin
Adsorption kinetics
Titania
Hydroxyapatite

ABSTRACT

The bioactivity of an implant is displayed on its ability to induce heterogeneous nucleation of biogenic apatite onto its surface upon immersion in body fluids; forming, through this layer, a stable bond with the host tissue. The present article evaluates the bioactivity of different nanostructured substrates based on synthetic hydroxyapatite (HA) and titania (TiO_2) nanoparticles, where we extend the debate regarding the selective roles played by the presence of albumin on the biogenic apatite coating evolution. The substrates bone-bonding potential was evaluated by keeping the materials in contact with Simulated Body Fluid, while the influence of the presence of Bovine Serum Albumin in bioactivity was analyzed by a spectrophotometric technique. Our results show that materials' surface reactivity and their interfacial hydration are responsible for the bonding-site alteration and surface charge density distribution, which in turn, regulate the protein adsorption process. As a matter of fact, variations on the protein adsorbed density have a directly proportional impact on calcium binding sites, which should be responsible for the initiation of the mineralization process, disturbing the deposition of the interfacial calcium phosphate (Ca-P) mineralized coating.

1. Introduction

A central stage in the osseointegration progression of a graft seems to be the spontaneous nucleation of a bone-like apatite layer

* Corresponding author.
E-mail addresses: nldelia@inquisur-conicet.gob.ar (N.L. D'Elia), noel.gravina@uns.edu.ar (N. Gravina), juanm.ruso@usc.es (J.M. Ruso), josemarcobrown@gmail.com (J.L. Marco-Brown), jmsieben@uns.edu.ar (J.M. Sieben), pmessina@uns.edu.ar (P.V. Messina).
[1] N.L. D'Elía and N. Gravina contributed equally to this work.

http://dx.doi.org/10.1016/j.jcis.2017.01.047
0021-9797/

on its surfaces in contact with biological fluids [1,2]. Numerous investigations detail the process that occurs at the foreign material surface by examining its *in vitro* apatite-forming ability after immersion on an acellular and protein-free simulated body fluid (SBF), a solution with ion concentrations almost equal to those of human blood plasma [3,4]. However, *in vivo* apatite formation depends on the complex and unknown chemical events occurring at the substrate – body fluids interface, which are likely to be influenced by the adhesion of soluble proteins. Actually, soluble proteins from blood and interstitial liquids are immediately adsorbed on materials' surfaces after being implanted [5,6], creating a coating that could be different from its original exterior shell and, thereby, giving it a unique biological identity. This layer plays a leading but controversial role in the biogenic apatite deposition process and in the future acceptance of the implant. Therefore, if the adsorbed proteins are correctly presented, they can stimulate a positive host tissue response, favoring wound repair and integration; whereas proteins adsorbed in a distorted state may incite the rejection or encapsulation of the foreign material [7–9]. As a matter of fact, for the functional design of an implantable device, it's essential to portray the communications among soluble proteins and its solid surface. Essentially three soluble proteins interact with blood-contact grafts: albumin, immunoglobulin G, and fibrinogen [10]. Of these, albumin is the most abundant human body extracellular protein; maintaining colloidal osmotic pressure in plasma, carrying insoluble components [11] and is the major calcium-binding protein present in the blood exhibiting up to 19 calcium binding sites on its imidazole groups [12]. Also, it is known to be the first to surround foreign bodies when they are in contact with blood and "passivating" their surfaces, blunting both pro-inflammatory and thrombogenic responses [13,14]. Literature findings also remark that albumin is the main protein involved in the bioactive glass adsorption [15,16] and, that it is a potent facilitator of mesenchymal stem cells colonization on mineralized human bone allografts [17]. Among materials used for calcified tissue replacement, Ca-P bioceramics and titanium (Ti) derivatives are believed to be the most biocompatible [18]. In previous works [19–22] we have formulated different materials based on nanoparticles: (i) biomimetic hydroxyapatite (HA) nano-rods [19,20] and (ii) TiO_2 nano-cuboids [21,22]. All samples have been proved to provide, *in vitro,* appropriate physical-chemical attributes to attain bone repair; including bioactivity [19–22]. Here, our investigation was extended by assessing the interaction of the previously mentioned nanostructured materials with albumin in order to check the protein's effect in the biomineralization process. To achieve this goal, a rigorous inspection of the evolution of a biologically active apatite coating in the presence of the protein was correlated with the biomolecules' adsorption-desorption isotherms. Particular attention is paid to the materials' surface reactivity, topography and their interfacial hydration. The regulation of tissue-implant interactions through biomolecules is still in its infancy, but early studies denote the value of this methodology for controlling cell and matrix events at the bone-implant boundaries [9,23,24]. The information derived from this work can improve the understanding about graft-fluids interface's mineralization process, and lead to the development of a successfully engineered bone tissue framework.

2. Experimental section

2.1. Reagents

Hexadecyl-trimethyl ammonium bromide (CTAB, 99% Sigma), *n*-heptane (Merck), butyl alcohol (ButOH, Merck,), cerium valerate ($Ce(Val)_3$,), titanium (IV) isopropoxide (TTIP, $Ti(IV)(OiPr)_4$, 97% Aldrich), poly (propylene glycol) (PPG, Sigma-Aldrich), sodium phosphate (Na_3PO_4, 96% Sigma), calcium chloride ($CaCl_2$, 99% Sigma), sodium nitrite ($NaNO_2$, 97% Sigma), sodium chloride (NaCl, 99,5% Sigma), sodium bicarbonate ($NaHCO_3$, 99,5% Sigma-Aldrich), potassium chloride (KCl, 99,5% Sigma-Aldrich), di potassium phosphate tri-hydrate ($K_2HPO_4{\cdot}3H_2O$, 99% Sigma-Aldrich), di-basic sodium phosphate (Na_2HPO_4, 99, 95% Sigma-Aldrich), magnesium chloride hexa-hydrate ($MgCl{\cdot}6H_2O$, 98% Sigma-Aldrich), sodium sulfate (Na_2SO_4, 99% Sigma-Aldrich), chloride acid (HCl, 30.0–34.0% Cicarelli), sodium hydroxide (NaOH, 97%, Sigma-Aldrich), tris(hydroxymethyl)aminomethane hydrochloride (Tris-HCl, 99% Sigma-Aldrich), phosphate buffer saline (PBS tablets, Na_2HPO_4/NaH_2PO_4, Sigma-Aldrich) and Bovine Serum Albumin (BSA, Fraction V, MW $\approx$ 66,000 g mol^{-1}, 95% Carl Roth) were used without further purification. For solutions preparation, only triplet-distilled water was used.

2.2. Substrates: HA, TiO_2, Ce-doped TiO_2 and CeO_2-doped TiO_2

Bone-like HA nano-rods (8 ± 1 nm diameter and 28 ± 3 nm length) with an isoelectric point (IP) of 3.1–3.4, as well as TiO_2, Ce-TiO_2 and CeO_2-TiO_2 tetragonal nanoparticles (with average particle sizes of 40, 34 and 28 nm respectively) with IPs of 5.0–5.2, were made as previously described [19–21], Fig. 1.

2.2.1. Structural characterization

The morphology of the substrates was observed via transmission electron microscopy (TEM). Micrographs were obtained on a Philips CM-12 TEM with an accelerating voltage of 120 kV. Observations were made in a bright field. Powdered samples were placed on cooper supports of 2000 mesh. The surface and porosities of TiO_2, Ce-doped TiO_2, CeO_2-doped TiO_2 [21] and HA nano-rods, see Figs. SM1 and SM2, were measured through nitrogen adsorption–desorption experiments as was previously described [21]. Textural characteristics for all samples are summarized in Table SM1.

2.2.2. Surface acidity (S_{Ac}) assay

The surface acidity was estimated by a titration method following the procedure developed by Tamele [25], to this 300.0 mg of nano-materials powder were dispersed in 40 ml of benzene by sonication throughout 30 min and stirring for another 30 min. After that five drops of 0.05 N Methyl Red (pKa = +4.8, H0 $\leqslant$ +4.8) solution in benzene were added to the beaker. Then *n*-butylamine (0.01 N) was titrated against the powder, and the amount of titer required to produce the color change on the surface of the powder was registered. The surface acidity associated to the hydroxyl concentrations of the samples was expressed in mmol per gram of sample.

2.2.3. Near infrared spectroscopy

A Nicolet iS50 FTIR – NIR spectrophotometer (Thermo Scientific, Waltham, MA, USA) along with a diffuse reflectance accessory (DRA, also called an integrating sphere) was used to measure the reflectance properties of the powders. The spectra were obtained in air atmosphere and at RT. In the present study the integrating sphere was operated in the reflectance mode in the region of 1000–2500 nm. A Gold NIR Diffuse Reflection Standard (99.9% Reflective) was used as a reference to calibrate the baseline. The powder samples were supported inside flat bottom glass vials to form pellets of 10 mm diameter and 5 mm thick for measurements.

2.3. Protein solution and adsorption experiment

The adsorption experiments were performed using bovine serum albumin (BSA), a "soft" globular protein with an IP of 4.6

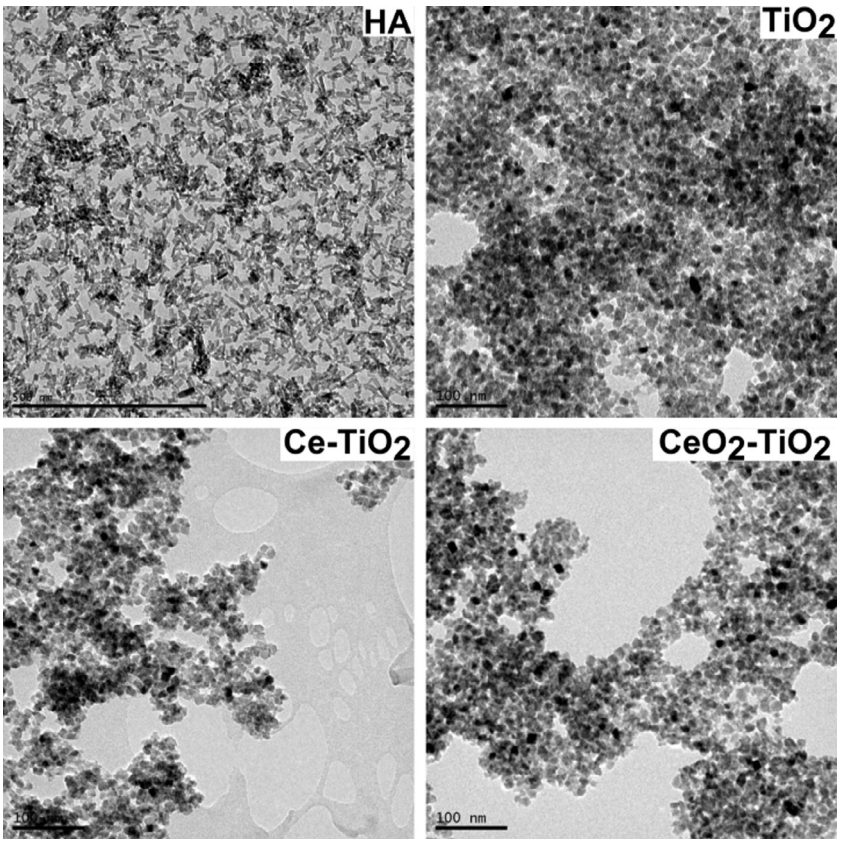

Fig. 1. Transmission electron microphotographs of the different nanoparticles used as BSA adsorption substrate. Scale bars: HA 500 nm; TiO_2, Ce-TiO_2 and CeO_2-TiO_2 100 nm.

[26], that is widely used as model system to study adsorption onto solid surfaces [16,26–28]. The day of each experiment protein solutions were freshly prepared by dissolving a known amount of the protein in PBS (pH = 7.4), gently stirring for 60 min. Phosphate was preferred than other organic buffers, i.e. Tris-HCl, because inorganic phosphate is abundant in biological environment [29] and on the other hand small organic molecules can be co-adsorbed and interfere on the experiments [30]. The BSA stock solution (4 mg mL^{-1}) was stored at 4–8 °C and diluted as required. Before the beginning of each experiment, BSA solutions were exposed to room temperature (RT) for a maximum of 1 h. Adsorption experiments (in darkness to avoid photodegradation) were carried out *in situ* in an UV–vis-NIR scanning spectrophotometer (Varian Cary 100 Bio) provided with a temperature controller (UV09005M013) using a 1 cm path length quartz cell. For this, 20 mg of adsorbent were place in contact with 2 mL of 4, 2 and 1 mg mL^{-1} BSA solutions at 37 °C. Adsorption measurements of the supernatant were taken every 0.4 min at λ = 278 nm following the emission of Tryptophan (Trp) group, ε = 43,824 M^{-1} cm^{-1} [31]. The range of concentrations used was within the linear range of the instrument, for details see Fig. SM3 of supporting material (SM). Mass balance was applied to calculate the amount of protein adsorbed on nanostructured materials, normalized per substrate surface area. This procedure allows avoiding problems associated with free protein adsorption sites available. The adsorbed density, Γ (μg dm^{-2}) was calculated with the following equation:

$$\Gamma = \frac{(C_0 - C)\,V}{m} S_{BET} \quad (1)$$

where C_0 is the protein initial concentration, C the residual concentration at time t, V is the solution volume, m is the adsorbent mass and S_{BET} is the Brunauer-Emmet-Teller (BET) surface area. The obtained curves were highly reproducible: each experiment was conducted three times, the standard deviation on Γ was estimated to be 0.01 μg m^{-2}.

2.4. Effect of BSA adsorption on the co-precipitation of biogenic apatite

2.4.1. Bioactivity assay

To evaluate the scaffolds bone-bonding potential, the materials were kept in contact with simulated body fluid (SBF) which has a ionic concentration similar to that of human plasma, containing Na^+ (142.0 mM), K^+ (5.0 mM), Mg^{2+} (1.5 mM), Ca^{2+} (2.5 mM), Cl^- (148.8 mM), HCO_3^- (4.2 mM), HPO_4^{-2} (1.0 mM) and SO_4^{-2} (0.5 mM). Following the standard procedure described by Kokubo et al. [32], 5 mg of each material were placed in polyethylene tubes with 3 mL of 1.5 × SBF solution and incubated in a water bath (37 ± 0.1 °C) for 10 days. After the incubation period, the specimens were removed from fluid, rinsed with distilled water and oven dried at 40 °C until constant weight was reached. As negative controls two conditions were simultaneously evaluated: on the one hand the 1.5 × SBF solution was kept in a polyethylene tube equal to those used in the test and the assay was considered valid while no precipitates were found; on the other hand, a negative bioactivity control was performed using a sample of pure commercial Anatase (AA) which was treated under the same conditions [33].

2.4.2. Bioactivity assay in presence of BSA

To evaluate the effect of the presence of BSA in the study of bioactivity, two experimental conditions were tested: (i) one in which 1 mg mL^{-1} of protein was dissolved in SBF following the previously described protocol and, (ii) another in which the albumin was pre-adsorbed on materials up to equilibrium time before

immersion in SBF. The stability of the protein solution was monitored spectrophotometrically by verifying the absence of changes in the BSA UV–vis spectrum recorded at the beginning and at the end of the assay, Fig. SM4, and the stability of pH thought the experiment (data not shown).

2.4.3. Structural characterization of the Ca-P mineralized coating

Surface morphology was evaluated using a field emission scanning electron microscope (ZEISS FE-SEM ULTRA PLUS). To acquire all the SEM images a secondary electron detector was used. The accelerating voltage (EHT) applied was 3.00 kV with a resolution (WD) of 2.1 nm. Local compensation of charge (by injecting nitrogen gas) was applied avoiding the sample staining. The associated X-ray energy-dispersive (EDX) spectrophotometer provided qualitative information about surface elemental composition microanalysis.

2.5. Statistical analysis

All experiments were conducted at least three times and all values were reported as the mean ± standard deviation (SD). Statistical analysis was carried out by the one-way analysis of variance (one-way ANOVA). The statistical difference between two sets of data was considered significant when $p < 0.05$.

3. Results and discussion

3.1. Nature and evolution of protein-substrate interfacial processes

3.1.1. Protein coating

Since physiological systems are highly dynamic, it is important to obtain a time-resolved knowledge of protein-coating formation on nano-sized surfaces. The adsorption kinetics process is sensitive to the interfacial structure even when the film is far from thermodynamic equilibrium [30,34], allowing a quantitative analysis of the structural evolution of the adsorbed layer, and eventually, a predictive capacity.

The time evolution of BSA adsorbed density (Γ/μg dm^{-2}) in contact with the tested nanostructured materials, Fig. 2, were analyzed. There is about 13.8 mg of albumin mL^{-1} in bone tissue fluids [35]; therefore different initial protein concentrations, C_0, were assessed for adsorption experiments. No significant change in concentration was detected for $C_0 > 1$ mg mL^{-1}, therefore only results obtained for $C_0 = 1$ mg mL^{-1} are shown. The shape of an adsorption isotherm can yield evidence about the affinity of adsorbing species toward the surface as well as the maximum equilibrium surface concentration.

Under physiological conditions, pH = 7.4, both BSA and the solid surfaces have a net negative charge that explains the Γ values within the range of micrograms of BSA per m^2 of substrate, Fig. 2. Even under unfavorable electrostatic interactions, adsorption's equilibria were attained after approximately 1 h of system evolution, undoubtedly due to specific substrate-protein sites contacts. The overall adsorption process appears to occur in a stepwise fashion with an initial rapid adsorption followed by a single plateau representing a pseudo-stable state. No BSA desorption can be detected under the selected experimental conditions. BSA kinetic adsorption curves were adjusted using the Avrami's exponential function [36–38]:

$$\Gamma(t) = \Gamma_{eq}\left(1 - \exp^{-[k_{av}t]^n}\right) \quad (2)$$

where k_{av} is the Avrami's kinetic rate constant and n is the reaction order. This equation do not consider the Langmuir's equation assumptions [39], and allows us to study in a simpler manner many events that are present in the kinetic adsorption of proteins: possible changes of the adsorption rates in function of the initial supernatant solution concentration and/or the adsorption time, as well as the determination of fractional kinetic orders [30]. To quantitatively compare the applicability of the selected kinetic model, the normalized standard deviation ($\Delta\Gamma(\%)$) was also calculated; $\Gamma(t)_{calc}$ is the adsorbed density value computed from the Avrami's model and a is the number of experimental points of the kinetic curve.

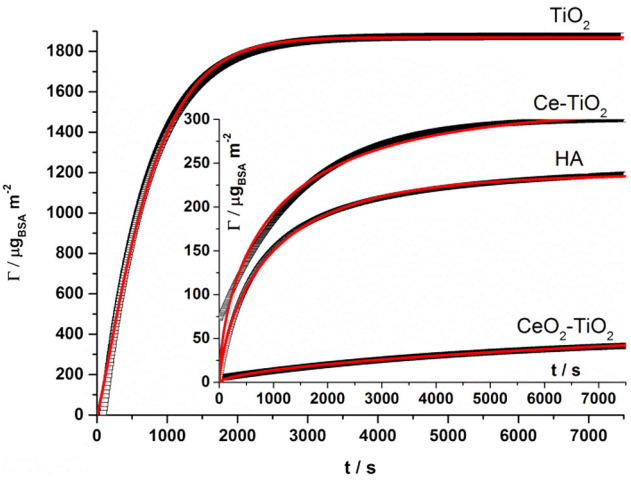

Fig. 2. BSA adsorption profiles at 37 °C on different nanostructured materials. $C_0 = 1$ mg mL^{-1}. Red line: Avrami's exponential function fitting.

$$\Delta\Gamma(\%) = 100 \times \sqrt{\frac{\sum\left[(\Gamma(t)_{\exp} - \Gamma(t)_{cal})/\Gamma(t)_{\exp}\right]^2}{a-1}} \quad (3)$$

Details of the kinetic constants and saturation values for BSA adsorption onto the different substrates were summarized in Table 1, in all cases $\Delta\Gamma(\%) \approx 0.05$ confirming the applicability of the selected kinetic model. As it was expected, the order (n) and the Avrami's kinetic constant (k_{av}) are dependent on the substrate identity. Despite of its low surface area ($S_{BET} = 3.0$ m^2 g^{-1} [21]), the TiO_2 substrate exhibited the highest equilibrium adsorbed density. Likewise, the initial absorption rate (v) and kinetic order for the BSA-TiO_2 adsorption were superior to the kinetic parameters obtained for the rest of the materials. The presence of cerium atoms, particularly the incorporation of CeO_2 nanoparticles, on the TiO_2 structure drastically reduced the adsorption kinetic parameters and the equilibrium adsorbed density. Moreover, the HA substrate despite having the highest surface area, $S_{BET} = 80.0$ m^2 g^{-1}, presented an insignificant protein adsorbed density at the equilibrium in comparison with its TiO_2 counterpart. Detailed analysis of dilute BSA solutions yields that the molecule acquires a prolate ellipsoidal shape (a = b < c) with a = b = 4 nm and c = 14 nm [26]. Assuming that the prolate ellipsoid molecule is confined within a parallelepiped of a = b = 4 nm side and c = 14 nm high, and that it can be situated parallel or perpendicular to the adsorbent surface without denature, the theoretical equilibrium adsorbed density necessary to complete a monomolecular layer of protein on the adsorbent would be about 1973 and 6900 μ_{BSA} m^{-2} respectively. This analysis evidence that the theoretical equilibrium adsorbed density value obtained for a monolayer of BSA extended parallel onto the adsorbent's surface is similar to the respective experimental value obtained for the protein adsorption on TiO_2 substrate. The obtained Γ experimental values for BSA adsorption on the rest of the materials are much lower than the theoretical ones; thus indicating that a monomolecular but incomplete layer is formed. This fact corresponds to the existence of different processes controlling the adsorption rate and it is not only a surface area dependent mechanism. Similar results were obtained in a previous work [30]

Table 1
Avrami's kinetic parameter.

Sample	$v/\mu g\ m^{-2}\ s^{-1}$	k_{av}/s^{-1}	n	$\Gamma_{eq}/\mu g_{BSA}\ m^{-2}$	R^2
TiO_2	2.258 ± 0.028	$(7.87 \pm 0.02) \times 10^{-2}$	$1.2 \pm 6.0 \times 10^{-3}$	$1.9 \times 10^{3} \pm 1.0$	0.996
Ce-TiO_2	0.116 ± 0.001	$(7.74 \pm 0.09) \times 10^{-2}$	$0.6 \pm 5.6 \times 10^{-3}$	315.8 ± 1.0	0.986
CeO_2-TiO_2	$(8 \pm 0.02) \times 10^{-3}$	$(0.18 \pm 0.03) \times 10^{-2}$	$0.6 \pm 6.0 \times 10^{-3}$	150 ± 1.3	0.997
HA	0.217 ± 0.004	$(7.94 \pm 0.02) \times 10^{-2}$	$0.7 \pm 2.2 \times 10^{-3}$	240 ± 0.2	0.998

and are related to the comparable dimensions of protein molecule and nanoparticle [5].

The different amount of adsorbed protein could be explained by a dissimilarity of the preferential bindings sites on the substrate surface; acidic proteins, including albumin, bind to HA surface through Ca-bridging sites [40] while Ti surfaces do not have specific binding sites. To understand the protein-nanomaterials association and to enlighten the different interaction mechanisms involved during adsorption kinetic regime that control the adsorption's rate, it is necessary to resort to additional detailed models which are analyzed below.

3.1.2. Mechanism of protein's interfacial transport

It is usually accepted that a typical liquid/solid adsorption process involves mass action as well as film and intra-particle diffusion pathways [41]. For physical adsorptions, the mass action is a very rapid process and can be negligible in a kinetic study. Thus, the kinetic process of adsorption is always controlled by liquid film or intra-particle diffusion [42]. Several diffusion models were tested in this work, such as: the "linear driving force" rate law [43] which is typically applied to describe the mass transferred thought the liquid film; the film diffusion mass transfer rate equation presented by Boyd et al. [44]; the homogeneous solid diffusion model [45]; Weber-Morris' model [46]; Dumwald-Wagner's model [47] and double-exponential function model proposed by Wilczak and Keinath [48]. Suitable results were obtained after the application of film and intra-particle diffusion models proposed by Boyd [44] and Weber–Morris [46] respectively, details were shown in SM**.** Boyd's diffusion model provides accurate results to describe the initial adsorption step for BSA interaction with titania based materials, Fig. 3 insert, suggesting that when BSA aqueous solution is placed in contact with these nanoparticles under static conditions the thickness of the boundary layer surrounding the particle should be significant and the boundary layer resistance or film diffusion should be the major driven rate-controlling factor for the initial adsorption [43]. However, the adsorption process onto the HA substrate was best fitted to the Weber and Morris' model, indicating that the migration of BSA within the intraparticle voids of the nano-HA substrate is the rate controlling step, Fig. SM7 insert. Results are summarized in Table 2.

Regardless of the diffusion model applied, the graphs do not pass through the origin, which means that the intraparticle and/or film diffusion mechanism are not the only rate controlling stage. Taking into account the inhomogeneous nature of proteins adsorption process [27,28] we considered the possibility of any kind of chemical interaction between adsorbed and pre-adsorbed molecules. So, reaction models were tested [49–52] obtaining good results only by the application of Elovich's equation [51,52], for details see SM, that is satisfied in chemical adsorption processes and is suitable for systems with heterogeneous adsorbing surfaces. Fig. 3 shows the kinetic regimes associated to BSA adsorption process onto TiO_2 substrate; complementary information regarding the kinetic BSA adsorption regimes onto Ce-TiO_2, CeO_2-TiO_2 and HA materials are shown in Figs. SM5–SM7. The presence of chemical reactions is in accordance with the evident dissimilar adsorption mechanisms on HA and titania based materials. To achieve an acceptable explanation we must explore deeper inside to the nature of the substrate surface reactivity and the adsorption process in solution.

3.1.3. Surface–site reactivity: Water vs. protein antagonism

The surface of a metal oxide can be represented as a bidimensional array of acid-base centers, quantifying the strength of these groups by the surface acidity (S_{AC}) parameter. The cationic metal centers act as Lewis acid sites while the anionic oxygen centers act as Lewis bases. Surface hydroxyl groups are able to serve as Brønsted acid or base sites as they are able to donate or accept a proton. The strength and the amount of Lewis and Brønsted acid-base sites will determine the reactivity of metal oxides surface, and should influence the substrate's adsorption capacity. In addition, the surface of most metal oxides will be hydrated in solution to some extent. The more or less ordered arrangement of H_2O molecules at the solid biomaterial surface also affect the surface reactivity and is expected to play a key role in biomaterials-body fluids interfacial events.

In previous works [20,22] we have determined that all materials had different water affinity, Fig. 4a. Specifically, on the surface of TiO_2 nanomaterials, a monomolecular layer of H_2O is initially formed on the activated surface by chemisorption due to interaction with the cations on the surface and then is converted into stable —OH groups by neutralization of the electrical charge presented in these cations, Fig. 4c. The —OH groups behave as Brønsted acid sites because they are polarized by the surface charge. Beyond the —OH layer on the surface, there is about 50–300 multilayers of adsorbed H_2O molecules formed by physisorption [53]. At increased distance from the surface, these layers are less affected by the charge and hence display reduced polarity, i.e. acidity [53]. The measured S_{Ac} values for the set of titanium materials revealed a correlation with protein adsorption; pure TiO_2 nanoparticles with the highest surface acidity, and correspondingly the least hydrated surface, presented the fastest and highest protein adsorption capacity, Fig. 4b. As S_{Ac} decrease, since more water molecules can form hydrogen bonds directly to the surface, the competition between water and proteins for the adsorption sites augment and the overall process results in a reduction of initial adsorption rate and the protein adsorption capacity.

The BSA adsorption onto HA substrate exhibited a different process; HA displays the highest water adsorption, but the Lewis acidic strength of surface Ca^{2+} cations in HA (S_{Ac} = 0.061 ± 0.004 - mmol g^{-1}) is not enough to justified the obtained value [54]. Literature results [54,55] revealed that strongly adsorbed water at the HA surface can be produced by the presence of a network of H-bonds interacting with the basic oxygen atoms of PO_4^{-3} groups, Fig. 4d. As adsorption phenomena of BSA onto HA nanoparticles is attributed to electrostatic interaction between Ca^{2+} cation and PO_4^{3-} anion of HA nanoparticles with COO^- anion and NH_4^+ cation of BSA protein [28], respectively, the competition between water and protein molecules is evident. Many authors have shown that hydrophobic surfaces are ideal to promote adhesion of proteins [16] and in particular of BSA [56]; the results presented here are consistent with literature information. Additionally, it was also suggested that the capacity of protein binding on a substrate is directly related to its surface area and topography [57]. Since the

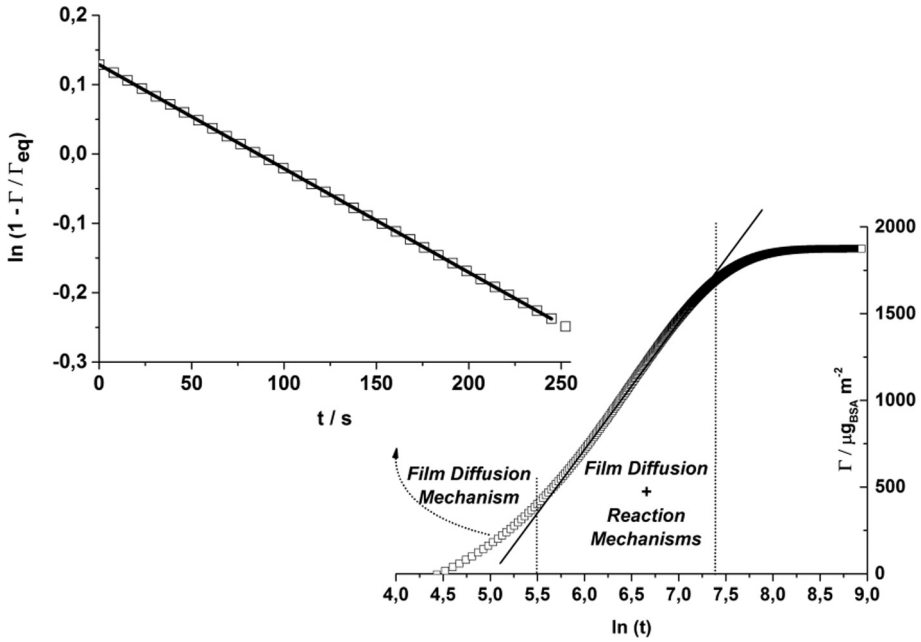

Fig. 3. Kinetic regimes associated to BSA adsorption process onto TiO_2 substrate.

Table 2
Diffusion and reaction mechanism parameters.

Sample	Diffusion models						Reaction models		
	Film diffusion			Intraparticle diffusion			Elovich's equation		
	$-R/s^{-1}$	$-I$	R^2	$k_{int}/s^{-½}$	I	R^2	$\alpha/\mu g\ m^{-2}$	$a/m^2\ \mu g^{-1}\ s^{-1}$	R^2
TiO_2	$(1.39 \pm 0.03) \times 10^{-3}$	0.07 ± 0.01	0.9987	66.05 ± 0.23	−617.5 ± 4.95	0.9987	729.67 ± 2.01	$(9.25 \pm 0.21) \times 10^{-6}$	0.9988
Ce-TiO_2	$(8.34 \pm 0.01) \times 10^{-4}$	−0.28 ± 0.01	0.9991	5.60 ± 0.01	35.31 ± 0.37	0.9984	74.28 ± 0.20	$(2.42 \pm 0.12) \times 10^{-4}$	0.9968
CeO_2-TiO_2	$(7.15 \pm 0.02) \times 10^{-5}$	−0.04 ± 0.02	0.9970	0.62 ± 0.01	−3.22 ± 0.04	0.9970	15.43 ± 0.05	$(1.71 \pm 0.21) \times 10^{-4}$	0.9910
HA	$(5.93 \pm 0.05) \times 10^{-4}$	−0.74 ± 0.01	0.9995	6.76 ± 0.03	−24.17 ± 0.46	0.9987	60.70 ± 0.11	$(2.68 \pm 0.05) \times 10^{-4}$	0.9991

investigated substrates exhibited similar roughness parameters [19,21] and specific surface is inversely related with the amount of adsorbed BSA, Fig. 4b, the results obtained in this study show that the surface hydrophobic effect on the protein adsorption is more significant than topographic features.

3.2. Mineralization process under the BSA coating effect

After 10 days of immersion in 1.5 × SBF, all tested substrates are capable to induce the formation of a spherulitic-like calcium deficient hydroxyapatite coating (cdHA, Ca/P = 1.56) similar to the mineral phase that exists in bone tissue [19,21], Fig. 5. Additionally, in view of the fact that hard tissue environment is more complex than *in vitro* solutions due to the role performed by the human plasma proteins, BSA effect on Ca-P layer deposition and morphology was evaluated, Fig. 5.

An intense protein adsorption, as it happens on the most hydrophobic substrate (TiO_2), results in a polymeric film covering almost the entire solid surface hindering the formation of the Ca-P layer, Figs. 5 and 6a. For Ce-doped TiO_2 substrates that exhibited lower protein adsorption capacity, the incubation of the materials in 1.5 × SBF with BSA (1 mg mL^{-1}) causes a spherulitic-like Ca-P (Ca/P = 1.56) coating formation; the protein adsorbs preferably onto Ca-P deposits once they are formed, Fig. 6b. The effect of protein adsorption on the nucleation process is intricate because this process can occur on the substrate and on the crystal nuclei, thus affecting interfacial tensions between crystal nuclei – liquid (γ_{CL}), substrate – crystal nuclei (γ_{SC}) and substrate –liquid (γ_{SL}); all these effects have different impacts on mineralization [58]. In accordance with the heterogeneous nucleation theory, the precipitation in presence of a foreign body, i.e. protein molecules, could induce a different process than those required for the homogeneous nucleation under a supersaturating media. These facts can be appreciated from the evaluation of the Gibbs free energy by the following equation [58]:

$$\Delta G_{het} = \varnothing \Delta G_{hom} \tag{4}$$

where $\varnothing = (2 + \cos\theta)(1 - \cos\theta)^2/4$ and, $\cos\theta = (\gamma_{SL} - \gamma_{SC})/\gamma_{CL}$. The presence of proteins in solution always decreases γ_{CL} and the formation of stable nuclei crystals will be easier in the presence of adsorbing proteins [58]. In our case, the BSA adsorption on hydrophobic substrates is higher than on the crystal nuclei; causing a superior decrease of the substrate-liquid interfacial tension (γ_{SL}) and thus lowering its nucleation ability [58]. Spherulitic deposits of Ca/P ≈ 2 can be appreciated onto Ce-TiO_2 and CeO_2-TiO_2 materials if BSA is pre-adsorbed on substrate instead of added to the SBF, Fig. 5. Again the protein effect is higher on the substrate that exhibits the maximum protein adsorption capacity. Physical-chemically, mineralization surfaces sustain dissolution–reprecipitation cascades as the result of exchanges at a solid–liquid interface in supersaturated conditions [59]. We have also observed BSA deposits onto Ca-P coatings even when the protein was pre-adsorbed on substrate, this fact indicates that the protein molecules are partially desorbed from the solid surface during their incubation in SBF and displaced from the surface by the growing Ca-P deposits, Fig. 6c and d.

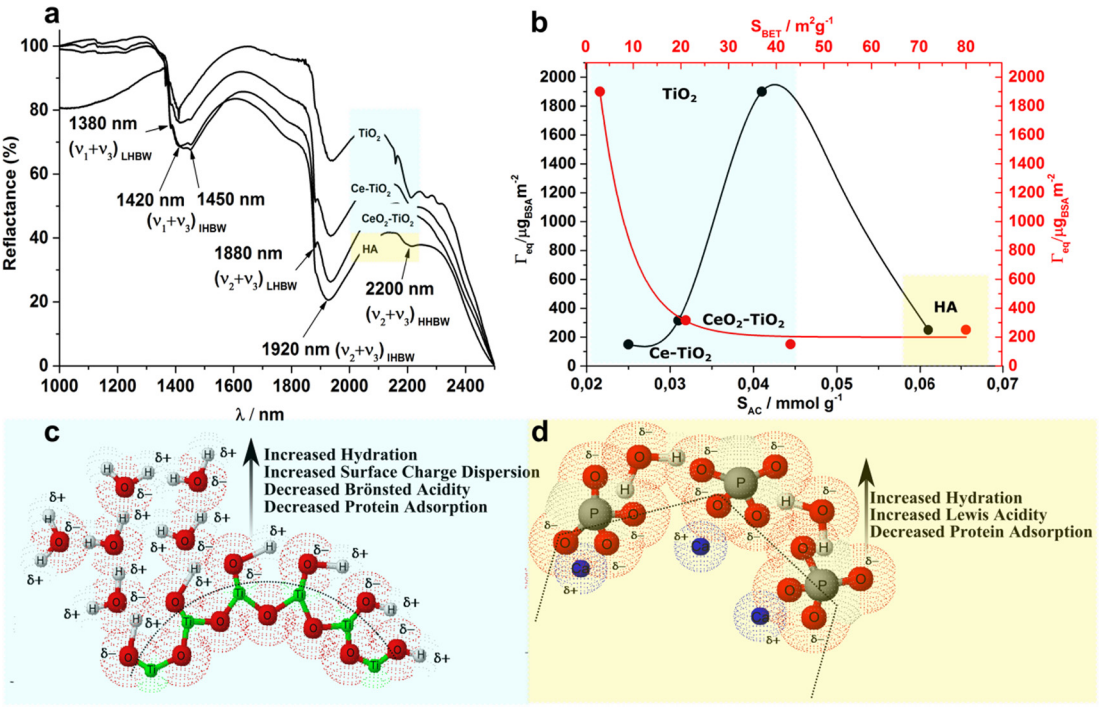

Fig. 4. (a) Near-infrared (NIR) spectra of H_2O molecules adsorbed on material surfaces. ν_1: symmetric stretching; ν_2: bending; ν_3: asymmetric stretching; LHBW: less hydrogen bonded water; IHBW: intermediate hydrogen bonded water; HHBW: high hydrogen bonded water. (b) BSA equilibria adsorbed density (Γ_{eq}/μg dm^{-2}) dependence on the substrate surface acidity (S_{AC}), black points, and surface area (S_{BET}), red points. Schematic representation of water layer molecules and charge dispersion onto (c) TiO_2, and (d) HA nano-sized surfaces.

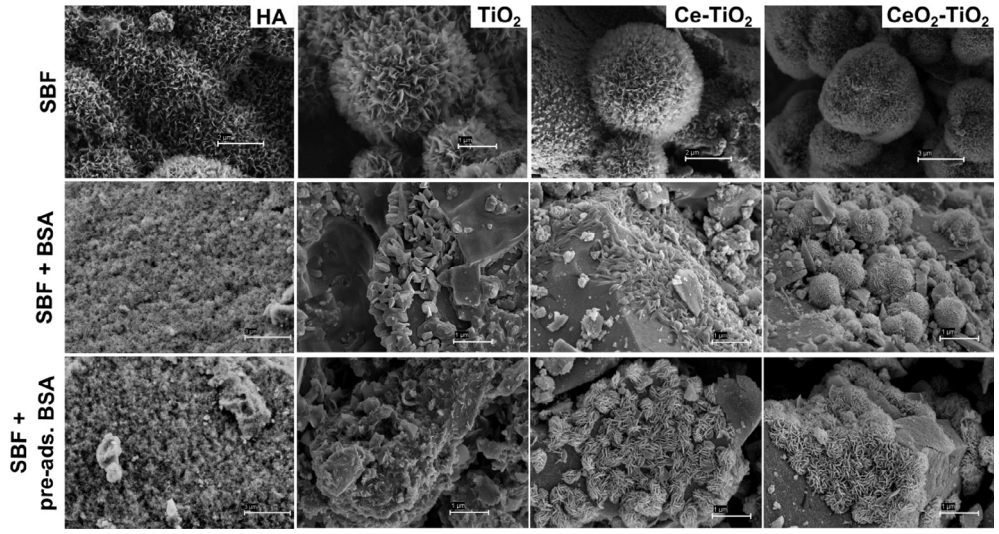

Fig. 5. SEM microphotographs of Ca-P coatings deposited on the different substrates after 10 days of incubation in: 1.5 SBF; 1.5 SBF with 1 mg mL^{-1} BSA and 1.5SBF after pre-adsorption of BSA.

Some authors conclude that protein addition in SBF does not change the basic thermodynamic nature of HA precipitation, but reduces the kinetic of crystal growth thought an augment of the ionic diffusion resistance due to the increased solution viscosity [60]. Our results reveal that, the specific BSA adhesion and the subsequent Ca-P coating formation are mostly influenced by the substrate identity and it is not only a matter of ionic diffusion resistance. EDX microanalysis demonstrated that in presence of BSA, the Ca^{2+} content on HA substrate is significantly reduced, being this effect more pronounced afterward protein was pre-adsorbed; please refer to Figs. SM8–SM14 for details. We assume that BSA has a double influence on mineralization of HA substrate, first the active-sites on mineral surface is efficiently coated by BSA slowing down the ionic diffusion to the crystal surface and secondly BSA leads to the calcium ion dissolution from HA surface reducing the co-precipitation of the new calcium phosphate layer.

4. Conclusion

In orthopedics, a key point in the formation of a stable tissue-implant union lies in the latter's ability to develop a bony-like calcium phosphate (Ca-P) coating on its surface [61]. In this work we

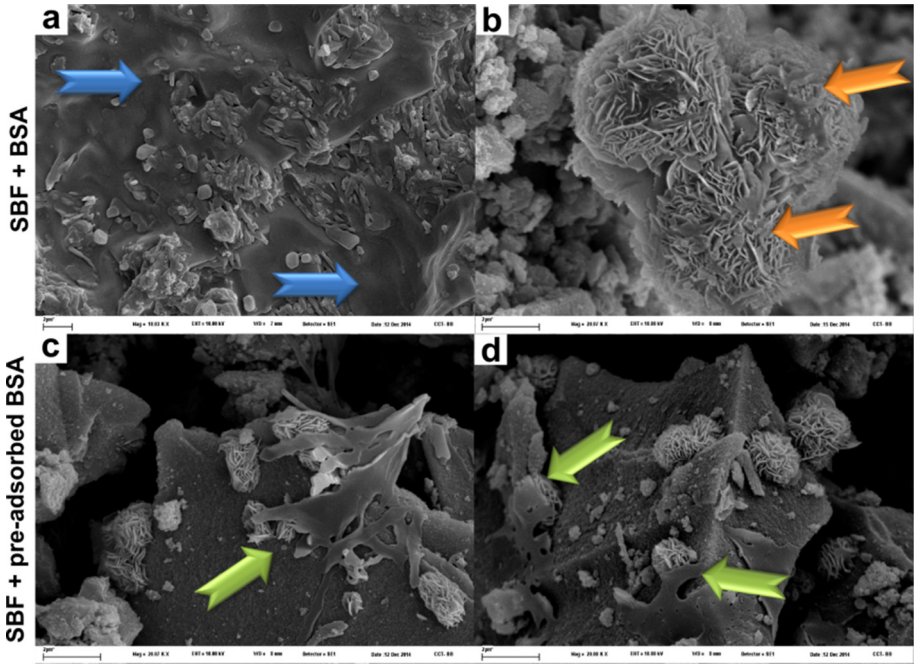

Fig. 6. (a) BSA coating covering the entire surface of hydrophobic substrate (TiO_2). (b) BSA deposition on Ca-P crystal globules. (c and d) BSA displacement by the crystal globules growth.

have analyzed the influence of BSA on the deposition of Ca-P coating onto different nanostructured materials from simulated body fluid (SBF) when the protein was incorporated into the solution. Hydroxyapatite (HA) and Ti derivatives (TiO_2 and Ce-TiO_2) surfaces were selected as substrate models because of their frequent use in the construction of calcified tissue replacement. Kinetic adsorption experiments were performed in order to understand the structural evolution of protein layer onto nano-sized substrates. It was shown that there was an unfavorable protein-substrate electrostatic interaction; however protein adsorption occurred on specific binding-sites. Theoretical adsorption kinetic models confirmed the existence of chemical reaction mechanisms controlling the adsorption rate. It was noted that albumin has a preferential adsorption onto hydrophobic surfaces and that effect is higher than nano-topography features. On the nanostructured TiO_2 surface, displaying the highest hydrophobicity and the least surface area, the protein extends parallel to create a complete monolayer; for the rest of the tested substrates a monomolecular but incomplete layer of BSA is formed.

Currently, the influence of plasma albumin on the mineralization process and on the subsequent graft osseointegration is a matter of controversy [62]. Our studies revealed that its presence in SBF hinders the nucleation of Ca-P crystals by blocking the contact sites among substrate reactive groups and Ca^{2+} ions from solution necessary to start the process of heterogeneous nucleation. This process is highly dependent of proteins adsorption preferences. Thus when the protein was pre-adsorbed on the materials' surfaces, the mineralization of the TiO_2 substrate was completely inhibited while Ce-doped TiO_2 surfaces showed signs of mineralization in the areas where there was no adsorbed protein. In addition, it was observed zones where the protein had been depleted from the surface due to the growth of Ca-P crystals. Obtained results demonstrated that mineralization occurs on the surface of the substrate and not on the layer of adsorbed protein, and that once the growing process starts, the Ca-P crystals are capable of displacing albumin from the substrate's surface. EDX microanalysis demonstrated that in presence of BSA, the Ca^{2+} content on HA substrate is significantly reduced. We assume that BSA has a double influence on mineralization of HA substrate: first the active-sites of the mineral surface are efficiently coated by BSA slowing down the ionic diffusion to the crystal surface and secondly BSA leads to the calcium ion dissolution from HA surface reducing the co-precipitation of the new calcium phosphate layer.

Albumin has a strong impact on the crystallization of Ca-P, and that is a fact beyond question. The overall results summarized in this work led us to conclude two main highlights. Firstly, being the most abundant blood protein, albumin will be present at the biomaterials-bone interface; hence we suggest that plasma proteins should be incorporated into the *in vitro* bioactivity assays using a complete simulated body fluid for a better reproduction of physiological conditions. Secondly, this article contributes to the discussion of the influence of BSA on the deposition of calcium phosphate deposits, demonstrating here that it plays an inhibitory role in the substrates studied.

Acknowledgements and funding sources

The authors acknowledge Universidad Nacional del Sur, Argentina (PGI 24/Q064), Concejo Nacional de Investigaciones Científicas y Técnicas de la República Argentina (CONICET, PIP – 11220130100100CO), Fundación Ramón Areces, Spain and Xunta de Galicia, Spain (AGRUP2015/11). NLD and ANG have doctoral fellowships of CONICET. PVM and JMS are independent and adjunct researchers of CONICET.

Appendix A. Supplementary material

Supplementary Material is available from the Elsevier Online Library: Substrates synthesis methods. N_2 adsorption – desorption isotherms and pore distribution of HA nano-rods. Kinetic adsorption models. X-ray energy dispersive (EDX) microanalysis. Supplementary data associated with this article can be found, in the online version, at http://dx.doi.org/10.1016/j.jcis.2017.01.047.

References

[1] P. Wang, L. Zhao, J. Liu, M.D. Weir, X. Zhou, H.H.K. Xu, Bone tissue engineering via nanostructured calcium phosphate biomaterials and stem cells, Bone Res. 2 (2014) 14017, http://dx.doi.org/10.1038/boneres.2014.17.

[2] M.G. Raucci, V. Guarino, L. Ambrosio, Biomimetic strategies for bone repair and regeneration, J. Funct. Biomater. 3 (2012) 688–705, http://dx.doi.org/10.3390/jfb3030688.

[3] T. Kokubo, S. Yamaguchi, Growth of novel ceramic layers on metals via chemical and heat treatments for inducing various biological functions, Front. Bioeng. Biotechnol. 3 (2015) 176, http://dx.doi.org/10.3389/fbioe.2015.00176.

[4] C. Bayram, M. Demirbilek, N. Çalışkan, M.E. Demirbilek, E. Baki Denkbc, Osteoblast activity on anodized Titania nanotubes: effect of simulated body fluid soaking time, J. Biomed. Nanotechnol. 8 (2012) 482–490, http://dx.doi.org/10.1166/jbn.2012.1391.

[5] M.S. Lord, M. Foss, F. Besenbacher, Influence of nanoscale surface topography on protein adsorption and cellular response, Nano Today. 5 (2010) 66–78, http://dx.doi.org/10.1016/j.nantod.2010.01.001.

[6] C.V. Vidal, A.I. Muñoz, Study of the adsorption process of bovine serum albumin on passivated surfaces of CoCrMo biomedical alloy, Electrochim. Acta 55 (2010) 8445–8452, http://dx.doi.org/10.1016/j.electacta.2010.07.028.

[7] A.E. Nel, L. Madler, D. Velegol, T. Xia, E.M.V. Hoek, P. Somasundaran, F. Klaessig, V. Castranova, M. Thompson, Understanding biophysicochemical interactions at the nano-bio interface, Nat. Mater. 8 (2009) 543–557, http://dx.doi.org/10.1038/nmat2442.

[8] N. Barnthip, P. Parhi, A. Golas, E.A. Vogler, Volumetric interpretation of protein adsorption: kinetics of protein-adsorption competition from binary solution, Biomaterials 30 (2009) 6495–6513, http://dx.doi.org/10.1016/j.biomaterials.2009.08.016.

[9] S. Tenzer, D. Docter, J. Kuharev, A. Musyanovych, V. Fetz, R. Hecht, F. Schlenk, D. Fischer, K. Kiouptsi, C. Reinhardt, Rapid formation of plasma protein corona critically affects nanoparticle pathophysiology, Nat. Nanotechnol. 8 (2013) 772–781, http://dx.doi.org/10.1038/nnano.2013.181.

[10] G. Khang, Evolution of gradient concept for the application of regenerative medicine, Biosurface Biotribol. 1 (2015) 202–213, http://dx.doi.org/10.1016/j.bsbt.2015.08.004.

[11] A. Farrugia, Albumin usage in clinical medicine: tradition or therapeutic?, Transfus Med. Rev. 24 (2010) 53–63, http://dx.doi.org/10.1016/j.tmrv.2009.09.005.

[12] A. Klinger, D. Steinberg, D. Kohavi, M.N. Sela, Mechanism of adsorption of human albumin to titanium in vitro, J. Biomed. Mater. Res. 36 (1997) 387–392. doi:10.1002/(SICI)1097-4636(19970905)36:3<387::AID-JBM13>3.0.CO;2-B.

[13] L. Tang, J.W. Eaton, Natural responses to unnatural materials: a molecular mechanism for foreign body reactions, Mol. Med. 5 (1999) 351.

[14] E. Missirlis, W. Lemm, Modern aspects of protein adsorption on biomaterials, Springer Sci. Business Media (2012), http://dx.doi.org/10.1016/0166-6622(92)80165-X.

[15] A.O. Paiva, N. Costa, S.C.P. Cachinho, M.H.V. Fernandes, Evaluation of the influence of albumin on the mineralization of a glass by Atomic Force Microscopy, J. Mater. Sci. - Mater. Med. 18 (2007) 599–604, http://dx.doi.org/10.1007/s10856-007-2307-3.

[16] K. Wang, C. Zhou, Y. Hong, X. Zhang, A review of protein adsorption on bioceramics, Interface Focus 2 (2012) 259–277, http://dx.doi.org/10.1098/rsfs.2012.0012.

[17] M. Weszl, G. Skaliczki, A. Cselenyák, L. Kiss, T. Major, K. Schandl, E. Bognár, G. Stadler, A. Peterbauer, L. Csönge, Z. Lacza, Freeze-dried human serum albumin improves the adherence and proliferation of mesenchymal stem cells on mineralized human bone allografts, J. Orthop. Res. 30 (2012) 489–496, http://dx.doi.org/10.1002/jor.21527.

[18] H. Zeng, K.K. Chittur, W.R. Lacefield, Analysis of bovine serum albumin adsorption on calcium phosphate and titanium surfaces, Biomaterials 20 (1999) 377–384, http://dx.doi.org/10.1016/S0142-9612(98)00184-7.

[19] N.L. D'Elía, A.N. Gravina, J.M. Ruso, J.A. Laiuppa, G.E. Santillán, P.V. Messina, Manipulating the bioactivity of hydroxyapatite nano-rods structured networks: effects on mineral coating morphology and growth kinetic, Biochim. Biophys. Acta – Gen. Subj. 2013 (1830) 5014–5026, http://dx.doi.org/10.1016/j.bbagen.2013.07.020.

[20] N.L. D'Elía, C. Mathieu, C.D. Hoemann, J.A. Laiuppa, G.E. Santillán, P.V. Messina, Bone-repair properties of biodegradable hydroxyapatite nano-rod superstructures, Nanoscale 7 (2015) 18751–18762, http://dx.doi.org/10.1039/C5NR04850H.

[21] A.N. Gravina, J.M. Ruso, J.A. Laiuppa, G.E. Santillán, J.L. Marco-Brown, N.L. D'Elia, P.V. Messina, Striped, bioactive Ce–TiO_2 materials with peroxynitrite-scavenging activity, J. Mater. Chem. B. 2 (2014) 834–845, http://dx.doi.org/10.1039/C3TB21556C.

[22] N. Gravina, K. Maghni, M. Welman, L. Yahia, D.A. Mbeh, P.V. Messina, Protective role against hydrogen peroxide and fibroblast stimulation via Ce-doped TiO_2 nanostructured materials, Biochim. Biophys. Acta – Gen. Subj. 2016 (1860) 452–464, http://dx.doi.org/10.1016/j.bbagen.2015.12.001.

[23] E.S. Place, N.D. Evans, M.M. Stevens, Complexity in biomaterials for tissue engineering, Nat. Mater. 8 (2009) 457–470, http://dx.doi.org/10.1017/CBO9781107415324.004.

[24] D.A. Puleo, R. Bizios, Biological interactions on materials surfaces: understanding and controlling protein, cell, and tissue responses, Springer Sci. & Business Media (2009), http://dx.doi.org/10.1007/978-0-387-98161-1.

[25] M.W. Tamele, Chemistry of the surface and the activity of alumina-silica cracking catalyst, Discuss. Faraday Soc. 8 (1950) 270–279, http://dx.doi.org/10.1039/DF9500800270.

[26] J.L. Wehmeyer, R. Synowicki, R. Bizios, C.D. García, Dynamic adsorption of albumin on nanostructured TiO 2 thin films, Mater. Sci. Eng., C 30 (2010) 277–282, http://dx.doi.org/10.1016/j.msec.2009.11.002.

[27] E. Mavropoulos, A.M. Costa, L.T. Costa, C.A. Achete, A. Mello, J.M. Granjeiro, A. M. Rossi, Adsorption and bioactivity studies of albumin onto hydroxyapatite surface, Colloids Surf. B. Biointerfaces. 83 (2011) 1–9, http://dx.doi.org/10.1016/j.colsurfb.2010.10.025.

[28] S.K. Swain, D. Sarkar, Study of BSA protein adsorption/release on hydroxyapatite nanoparticles, Appl. Surf. Sci. 286 (2013) 99–103, http://dx.doi.org/10.1016/j.apsusc.2013.09.027.

[29] C.F. Dick, A. Dos-Santos, #233, L. Ara, #250, jo, J. Meyer-Fernandes, Roberto, Inorganic phosphate as an important regulator of phosphatases, Enzyme Res. 2011 (2011) 7. http://dx.doi.org/10.4061/2011/103980.

[30] N. Hassan, A. Soltero, D. Pozzo, P.V. Messina, J.M. Ruso, Bioinspired templates for the synthesis of silica nanostructures, Soft Matter 8 (2012) 9553–9562, http://dx.doi.org/10.1039/c2sm26263k.

[31] F. Putnam, The Plasma Proteins V3: Structure, Function, and Genetic Control, Elsevier, 2012.

[32] T. Kokubo, H. Kushitani, S. Sakka, T. Kitsugi, T. Yamamuro, Solutions able to reproduce in vivo surface-structure changes in bioactive glass-ceramic A-W3, J. Biomed. Mater. Res. 24 (1990) 721–734, http://dx.doi.org/10.1002/jbm.820240607.

[33] P. Li, C. Ohtsuki, T. Kokubo, K. Nakanishi, N. Soga, K. de Groot, The role of hydrated silica, titania, and alumina in inducing apatite on implants, J. Biomed. Mater. Res. 28 (1994) 7–15, http://dx.doi.org/10.1002/jbm.820280103.

[34] Y. Tie, C. Calonder, P.R. Van Tassel, Protein adsorption: kinetics and history dependence, J. Colloid Interface Sci. 268 (2003) 1–11, http://dx.doi.org/10.1016/S0021-9797(03)00516-2.

[35] Repair and Remineralization, in: Hard Tissue Growth. Ciba Found. Symp., 1973, pp. 213–236.

[36] M. Avrami, Kinetics of phase change. I General theory, J. Chem. Phys. 7 (1939) 1103–1112, http://dx.doi.org/10.1063/1.1750380.

[37] M. Avrami, Kinetics of phase change. II transformation-time relations for random distribution of nuclei, J. Chem. Phys. 8 (1940) 212–224, http://dx.doi.org/10.1063/1.1750631.

[38] M. Avrami, Granulation, phase change, and microstructure kinetics of phase change. III, J. Chem. Phys. 9 (1941) 177–184, http://dx.doi.org/10.1063/1.1750872.

[39] I. Langmuir, The adsorption of gases on plane surfaces of glass, mica and platinum, J. Am. Chem. Soc. 40 (1918) 1361–1403, http://dx.doi.org/10.1021/ja02242a004.

[40] B. Feng, J. Chen, X. Zhang, Interaction of calcium and phosphate in apatite coating on titanium with serum albumin, Biomaterials 23 (2002) 2499–2507, http://dx.doi.org/10.1016/S0142-9612(01)00384-2.

[41] S. Karmaker, T. Sen, T.K. Saha, Adsorption of reactive yellow 145 onto chitosan in aqueous solution: kinetic modeling and thermodynamic analysis, Polym. Bull. 72 (2015) 1879–1897, http://dx.doi.org/10.1007/s00289-015-1378-4.

[42] H. Qiu, L. Lv, B. Pan, Q. Zhang, W. Zhang, Q. Zhang, Critical review in adsorption kinetic models, J. Zhejiang Univ. Sci. A. 10 (2009) 716–724, http://dx.doi.org/10.1631/jzus.A0820524.

[43] J.A. Chinn, S.M. Slack, Biomaterials: protein surface interactions, Biomed. Eng. Handbook. Boca Rat. 200 (2000) 1597–1608. CRC Press.

[44] G.E. Boyd, A.W. Adamson, L.S. Myers Jr, The exchange adsorption of ions from aqueous solutions by organic zeolites. II. Kinetics1, J. Am. Chem. Soc. 69 (1947) 2836–2848.

[45] D.O. Cooney, Adsorption Design for Wastewater Treatment, CRC Press, 1998.

[46] W.J. Weber, J.C. Morris, Kinetics of adsorption on carbon from solution, J. Sanit. Eng. Div. 89 (1963) 31–60.

[47] H. Dunwald, C. Wagner, Measurement of diffusion rate in the process of dissolving gases in solid phases, Z. Phys. Chem. (Leipzig) B. 24 (1934) 53–58.

[48] A. Wilczak, T.M. Keinath, Kinetics of sorption and desorption of copper (II) and lead (II) on activated carbon, Water Environ. Res. 65 (1993) 238–244.

[49] S. Lagergren, Zur Theorie der sogenannten Absorption gelöster Stoffe, PA Norstedt & söner, 1898.

[50] Y.-S. Ho, Review of second-order models for adsorption systems, J. Hazard. Mater. 136 (2006) 681–689, http://dx.doi.org/10.1016/j.jhazmat.2005.12.043.

[51] I.S. McLintock, The Elovich equation in chemisorption kinetics, Nature 216 (1967) 1204–1205, http://dx.doi.org/10.1038/2161204a0.

[52] S.H. Chien, W.R. Clayton, Application of Elovich equation to the kinetics of phosphate release and sorption in soils, Soil Sci. Soc. Am. J. 44 (1980) 265–268, http://dx.doi.org/10.2136/sssaj1980.03615995004400020013x.

[53] Y. Arai, Chemistry of powder production, Springer Sci. Business Media (2012), http://dx.doi.org/10.1007/978-94-009-1493-3.

[54] V. Bolis, C. Busco, G. Martra, L. Bertinetti, Y. Sakhno, P. Ugliengo, F. Chiatti, M. Corno, N. Roveri, Coordination chemistry of Ca sites at the surface of nanosized hydroxyapatite: interaction with H_2O and CO, Philos. Trans. R. Soc. London A Math. Phys. Eng. Sci. 370 (2012) 1313–1336, http://dx.doi.org/10.1098/rsta.2011.0273.

[55] Y. Pekounov, K. Chakarova, K. Hadjiivanov, Surface acidity of calcium phosphate and calcium hydroxyapatite: FTIR spectroscopic study of low-temperature CO adsorption, Mater. Sci. Eng., C 29 (2009) 1178–1181, http://dx.doi.org/10.1016/j.msec.2008.10.011.

[56] Y.L. Jeyachandran, J.A. Mielczarski, E. Mielczarski, B. Rai, Efficiency of blocking of non-specific interaction of different proteins by BSA adsorbed on hydrophobic and hydrophilic surfaces, J. Colloid Interface Sci. 341 (2010) 136–142.
[57] T. Kopac, K. Bozgeyik, Effect of surface area enhancement on the adsorption of bovine serum albumin onto titanium dioxide, Colloids Surfaces B Biointerfaces 76 (2010) 265–271.
[58] C. Combes, C. Rey, Adsorption of proteins and calcium phosphate materials bioactivity, Biomaterials 23 (2002) 2817–2823.
[59] L.C. Palmer, C.J. Newcomb, S.R. Kaltz, E.D. Spoerke, S.I. Stupp, Biomimetic systems for hydroxyapatite mineralization inspired by bone and enamel, Chem. Rev. 108 (2008) 4754–4783, http://dx.doi.org/10.1021/cr8004422.
[60] K. Wang, Y. Leng, X. Lu, F. Ren, X. Ge, Y. Ding, Theoretical analysis of protein effects on calcium phosphate precipitation in simulated body fluid, CrystEngComm 14 (2012) 5870–5878, http://dx.doi.org/10.1039/c2ce25216c.
[61] T. Kokubo, Bioactive glass ceramics: properties and applications, Biomaterials 12 (1991) 155–163.
[62] A.P. Serro, M. Bastos, J.C. Pessoa, B. Saramago, Bovine serum albumin conformational changes upon adsorption on titania and on hydroxyapatite and their relation with biomineralization, J. Biomed. Mater. Res. A. 70 (2004) 420–427, http://dx.doi.org/10.1002/jbm.a.30096.